Article

Cell Reports

Impairment of Inhibitory Synapse Formation and Motor Behavior in Mice Lacking the NL2 Binding Partner LHFPL4/GARLH4

Graphical Abstract

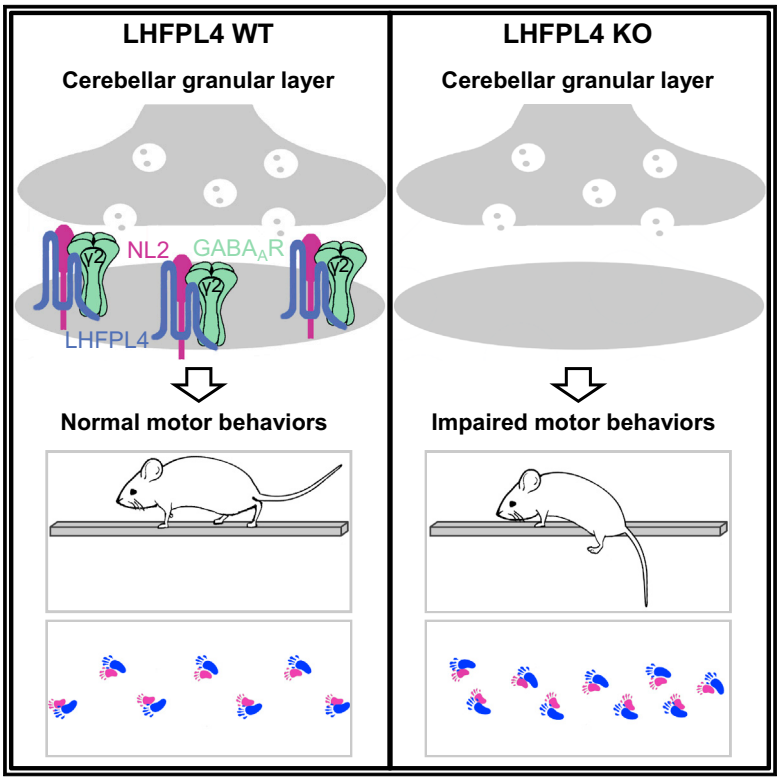

Highlights

- LHFPL4 is a major NL2 binding partner enriched at inhibitory postsynaptic sites
- LHFPL4 and NL2 regulate each other's protein levels and synaptic clustering
- Inhibitory synapse formation in the cerebellar granular layer depends on LHFPL4
- LHFPL4 is essential for motor behaviors and postnatal survival

Authors

Min Wu, Hong-Lei Tian, Xiaobo Liu, John Ho Chun Lai, Shengwang Du, Jun Xia

Correspondence

jxia@ust.hk

In Brief

Wu et al. identify LHFPL4/GARLH4 as a major NL2 binding partner that is specifically enriched at inhibitory postsynaptic sites and regulates inhibitory synapse formation. Deletion of LHFPL4/GARLH4 in mice results in profound impairment of inhibitory synapse formation as well as prominent motor behavioral deficits and premature death.

Wu et al., 2018, Cell Reports *23*, 1691–1705
May 8, 2018
https://doi.org/10.1016/j.celrep.2018.04.015

CellPress

Cell Reports
Article

Impairment of Inhibitory Synapse Formation and Motor Behavior in Mice Lacking the NL2 Binding Partner LHFPL4/GARLH4

Min Wu,[1] Hong-Lei Tian,[1] Xiaobo Liu,[1] John Ho Chun Lai,[1] Shengwang Du,[2] and Jun Xia[1,3,*]
[1]Division of Life Science and State Key Laboratory of Molecular Neuroscience, The Hong Kong University of Science and Technology, Clear Water Bay, Kowloon, Hong Kong, China
[2]Department of Physics, The Hong Kong University of Science and Technology, Clear Water Bay, Kowloon, Hong Kong, China
[3]Lead Contact
*Correspondence: jxia@ust.hk
https://doi.org/10.1016/j.celrep.2018.04.015

SUMMARY

Normal brain functions depend on the balanced development of excitatory and inhibitory synapses. Our knowledge of the molecular mechanisms underlying inhibitory synapse formation is limited. Neuroligin-2 (NL2), a transmembrane protein at inhibitory postsynaptic sites, is capable of initiating inhibitory synapse formation. In an effort to search for NL2 binding proteins and the downstream mechanisms responsible for inhibitory synapse development, we identify LHFPL4/GARLH4 as a major NL2 binding partner that is specifically enriched at inhibitory postsynaptic sites. LHFPL4/GARLH4 and NL2 regulate the protein levels and synaptic clustering of each other in the cerebellum. *Lhfpl4/Garlh4*$^{-/-}$ mice display profound impairment of inhibitory synapse formation as well as prominent motor behavioral deficits and premature death. Our findings highlight the essential role of LHFPL4/GARLH4 in brain functions by regulating inhibitory synapse formation as a major NL2 binding partner.

INTRODUCTION

Neurons in the central nervous system (CNS) process and transmit information predominantly through two distinct categories of synapses: glutamatergic excitatory synapses and γ-aminobutyric acid (GABA)ergic inhibitory synapses. α-amino-3-hydroxy-5-methyl-4-isoxazolepropionic acid (AMPA)-type glutamate receptors (AMPARs) mediate the majority of fast excitatory synaptic transmission, whereas ionotropic type A GABA receptors (-$GABA_A$Rs) mediate most of the fast inhibitory synaptic transmission in the CNS (Olsen and Sieghart, 2008; Traynelis et al., 2010). Normal brain functions depend on the balanced development of excitatory and inhibitory synapses, as demonstrated in studies of brain disorders such as epilepsy, autism, and schizophrenia (Foss-Feig et al., 2017; Fritschy, 2008; Hoftman et al., 2017; Krystal et al., 2017; Lee et al., 2017; Tatti et al., 2017). Thus, achieving a better understanding of the molecular mechanisms of synapse development through identifying the molecular organizers of both excitatory and inhibitory synapses could provide insight into brain disorders.

Synaptogenesis is a tightly regulated process involving three characteristic steps: target recognition and initial physical contact, presynaptic and postsynaptic component assembly, and maturation (Shen and Scheiffele, 2010; Siddiqui and Craig, 2011). To explore the molecular mechanisms of synapse formation, extensive studies have been conducted to identify protein components of the excitatory glutamatergic postsynaptic density (PSD) using either yeast two-hybrid (Y2H) screening or purification coupled with mass spectrometry analysis (Greger et al., 2017; Sheng and Kim, 2011). Hundreds of protein constituents in the excitatory PSD have been identified, including receptor proteins, receptor auxiliary proteins, adhesion molecules, scaffold proteins, cytoskeletal elements, and cytoplasmic signaling proteins (Greger et al., 2017; Sheng and Kim, 2011). In contrast, the protein list of currently known molecular organizers specific to the inhibitory PSD is sparse (Krueger-Burg et al., 2017). Given the diversity of $GABA_A$R subtypes and the complexity of interneurons (Kepecs and Fishell, 2014; Olsen and Sieghart, 2008), a large number of inhibitory synaptic proteins likely remain to be identified.

Neuroligin-2 (NL2) is well known for its specific role in inhibitory synapse formation and its function as a cell adhesion molecule (Chih et al., 2005; Graf et al., 2004; Varoqueaux et al., 2004). NL2 functions through *trans*-synaptic binding to its presynaptic partner neurexin as well as intracellular interactions with collybistin and the inhibitory postsynaptic scaffold protein gephyrin (Poulopoulos et al., 2009; Südhof, 2008). Functionally, NL2-deficient mice display increased neuronal excitability and behavioral defects caused by the reduction of synaptic gephyrin and $GABA_A$R clusters as well as impairment of inhibitory synaptic transmission (Babaev et al., 2016; Blundell et al., 2009; Chubykin et al., 2007; Gibson et al., 2009; Hoon et al., 2009; Jedlicka et al., 2011; Liang et al., 2015; Poulopoulos et al., 2009; Wöhr et al., 2013; Zhang et al., 2015). Furthermore, mutations in the NL2 (*Nlgn2*) gene have been reported to be associated with schizophrenia, anxiety, and autism in humans (Parente et al., 2017; Sun et al., 2011). Thus, NL2 is essential for the functional integrity of inhibitory synapses.

In this study, we sought to identify inhibitory PSD proteins associated with NL2. Using immunoprecipitation coupled with mass spectrometry analysis, we identified a four-transmembrane

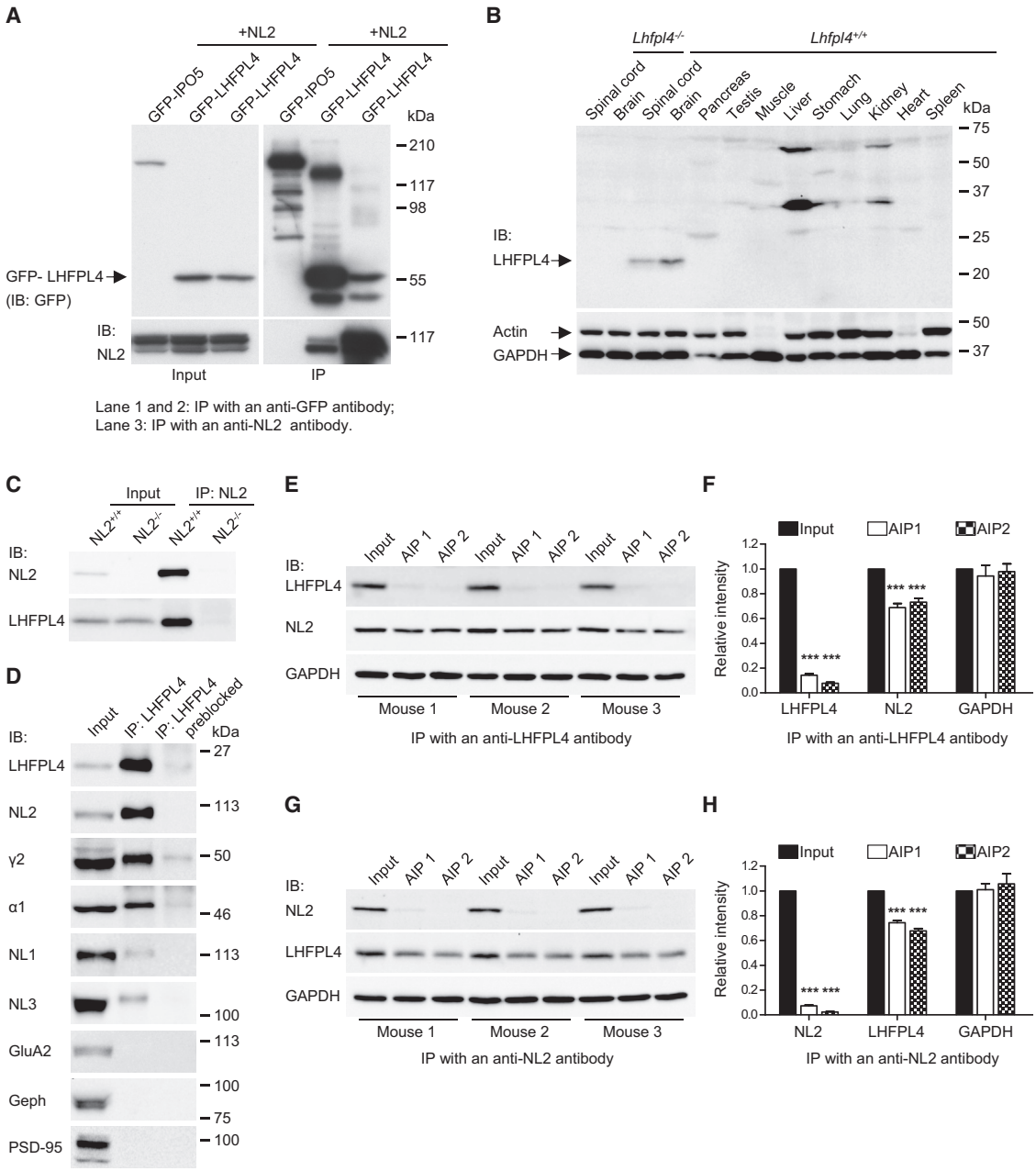

Lane 1 and 2: IP with an anti-GFP antibody;
Lane 3: IP with an anti-NL2 antibody.

Figure 1. LHFPL4/GARLH4 and NL2 Form Tight Complexes *In Vitro* and *In Vivo*

(A) Co-immunoprecipitation of GFP-LHFPL4 and NL2 in transfected HEK293T cells. An irrelevant protein, GFP-IPO5, was used as a negative control. IP, immunoprecipitation.

(B) In the mouse tissues examined, LHFPL4 Ab#1 detected the predicted band of approximately 22 kDa only in the brain and spinal cord.

(C) *In vivo* immunoprecipitation with an anti-NL2 antibody. LHFPL4/GARLH4 co-immunoprecipitated strongly with NL2 in brain homogenates from the WT mouse but not the NL2 KO mouse.

(D) *In vivo* immunoprecipitation with LHFPL4 Ab#1. LHFPL4/GARLH4 co-immunoprecipitated NL2, $GABA_AR$ γ2, $GABA_AR$ α1, and a small amount of NL1 and NL3. LHFPL4/GARLH4 did not co-immunoprecipitate GluA2, gephyrin (Geph), or PSD-95. NL2, $GABA_AR$ γ2, $GABA_AR$ α1, NL1, and NL3 were not pulled down when LHFPL4 Ab#1 was preblocked by the antigenic peptide.

(E) LHFPL4/GARLH4 was depleted from mouse brain homogenates by two consecutive immunoprecipitation experiments using LHFPL4 Ab#1. Input was defined as brain homogenates before immunoprecipitation. AIP1 and AIP2 were defined as brain homogenates after the first and second immunoprecipitation, respectively.

(F) Quantification of the protein level in (E). The chemiluminescence intensity of the input was normalized to 1. When LHFPL4/GARLH4 was almost completely depleted (7.77% ± 0.78% in AIP2), there was 73.21% ± 3.11% of NL2 left in AIP2 (n = 6 mice). Therefore, 29% of NL2 was associated with LHFPL4/GARLH4 in mouse brain homogenates.

(legend continued on next page)

domain protein, lipoma HMGIC fusion partner-like 4 (LHFPL4) (Longo-Guess et al., 2005; Petit et al., 1999) as a major NL2 binding protein. LHFPL4 is also termed $GABA_AR$ regulatory Lhfpl4 (GARLH4) because it has recently been reported to regulate the synaptic localization of $GABA_AR$ and inhibitory transmission (Yamasaki et al., 2017). We found that LHFPL4/GARLH4 is exclusively expressed in the nervous system and specifically enriched at inhibitory postsynaptic sites. Significant proportions of LHFPL4/GARLH4 and NL2 are associated with each other in the brain, and they regulate the protein levels and the synaptic clustering of each other in the cerebellum. Deficiency of LHFPL4/GARLH4 results in impairment of inhibitory synapse formation and motor behavior deficits as well as increased pentylenetetrazole (PTZ)-induced seizure susceptibility and premature death in *Lhfpl4/Garlh4*$^{-/-}$ mice.

RESULTS

Identification of LHFPL4/GARLH4 as a Major NL2 Binding Partner by Immunoprecipitation-Mass Spectrometry

To identify inhibitory synaptic proteins that interact with NL2, mouse brain homogenates were subjected to immunoprecipitation using an anti-NL2 antibody followed by mass spectrometry analysis. To improve the specificity, the same experimental procedures were conducted in parallel with brain homogenates from NL2 knockout (KO) mice. Only proteins identified in the immunoprecipitated products of brain homogenates from wild-type (WT) mice, but not those from NL2 KO mice, were considered to be specific NL2-interacting proteins. In addition, the experiments coupling immunoprecipitation with mass spectrometry (IP-MS) were repeated twice to obtain a list of NL2-interacting proteins with high confidence. Only proteins repeatedly identified in all three immunoprecipitation-mass spectrometry experiments were selected for further study. With these criteria, we confirmed the presence of well characterized inhibitory synaptic proteins in the NL2-associated protein complexes (Table S1), including gephyrin, collybistin, Magi2, and $GABA_AR$ subunits (α1, α2, α3, α6, β1, β2, β3, γ2, and γ3) (Olsen and Sieghart, 2008; Poulopoulos et al., 2009; Sumita et al., 2007). In addition, we identified LHFPL4/GARLH4 as an NL2 binding protein with high peptide counts (Table S1).

The interaction between LHFPL4/GARLH4 and NL2 was first verified by conducting *in vitro* co-immunoprecipitation experiments using transfected HEK293T cells. When LHFPL4/GARLH4 was pulled down, NL2 co-immunoprecipitated with LHFPL4/GARLH4 (Figure 1A, lane 2). In the reciprocal co-immunoprecipitation experiment, LHFPL4/GARLH4 co-immunoprecipitated with NL2 (Figure 1A, lane 3).

To study the endogenous LHFPL4/GARLH4 protein, we generated two rabbit anti-LHFPL4/GARLH4 antibodies: LHFPL4 antibody (Ab) #1 and LHFPL4 Ab#2. Both antibodies selectively recognized LHFPL4/GARLH4 but not other LHFPL4/GARLH4 homologs, including LHFPL 1, 2, 3, and 5 (Figures S1A and S1B). LHFPL4 Ab#1 detected a band with a predicted molecular weight of approximately 22 kDa in the mouse brain and spinal cord and cultured rat hippocampal neurons (Figure 1B; Figure S2B). In contrast, the band was undetectable in the brain and spinal cord from LHFPL4/GARLH4 KO mice (Figure 1B). LHFPL4 Ab#1 also detected a few other bands in non-neuronal tissues, such as the liver, but these bands were non-specific because they were still present in LHFPL4/GARLH4 KO mice (Figure S1C). The *in vivo* interaction between LHFPL4/GARLH4 and NL2 was then verified. We first used an anti-NL2 antibody to pull down NL2. LHFPL4/GARLH4 co-immunoprecipitated robustly with NL2 in brain extracts from WT mice but not from NL2 KO mice (Figure 1C). In the reverse direction, we used LHFPL4 Ab#1 to pull down LHFPL4/GARLH4. NL2 was found to co-immunoprecipitate strongly with LHFPL4/GARLH4 (Figure 1D). In the control experiment, NL2 was undetectable in the pull-down when LHFPL4 Ab#1 was preblocked by the antigenic peptide (Figure 1D, lane 3). A small amount of NL1 and NL3 also co-immunoprecipitated with LHFPL4/GARLH4 from mouse brain homogenates (Figure 1D).

Based on the protein amount in the input and immunoprecipitation samples (Figure 1D, lanes 1 and 2), approximately 30% of NL2 but only approximately 1% of NL1 and NL3 were estimated to be associated with LHFPL4/GARLH4. To quantify the percentages of NL2 and LHFPL4/GARLH4 that were associated with each other *in vivo*, we conducted quantitative co-immunoprecipitation. First, LHFPL4 Ab#1 was used to completely deplete LHFPL4/GARLH4 from the mouse brain homogenates by two consecutive immunoprecipitation experiments. By quantifying the chemiluminescence intensity of the resulting proteins on immunoblots, we determined that 29% of NL2 was depleted when LHFPL4/GARLH4 was completely depleted from the brain homogenates (Figures 1E and 1F). Similarly, 33% of LHFPL4/GARLH4 was depleted when NL2 was completely depleted from the brain homogenates using an anti-NL2 antibody (Figures 1G and 1H). These results suggested that 29% of NL2 was associated with LHFPL4/GARLH4, whereas 33% of LHFPL4/GARLH4 was associated with NL2 in the mouse brain. In addition, immunoprecipitation studies showed that LHFPL4/GARLH4 also co-immunoprecipitated $GABA_AR$ γ2 and α1 subunits but did not co-immunoprecipitate gephyrin, GluA2, or PSD-95 (Figure 1D). Taken together, we identified LHFPL4/GARLH4 as a major NL2 binding partner that is also associated with $GABA_ARs$.

LHFPL4/GARLH4 Is Specifically Enriched at Inhibitory Postsynaptic Sites

We subsequently examined the subcellular localization of LHFPL4/GARLH4. Endogenous LHFPL4/GARLH4 in primary cultured neurons immunolabeled by LHFPL4 Ab#1 exhibited a punctate pattern (Figures 2A and 2B) that resembled the localization pattern of inhibitory synapses. These puncta were undetectable in neurons infected with adeno-associated viruses (AAV)

(G) NL2 was depleted from mouse brain homogenates as described in (E) using an anti-NL2 antibody.
(H) Quantification of the protein level in (G). When NL2 was almost completely depleted (2.33% ± 0.42% in AIP2), there was 67.69% ± 1.88% of LHFPL4/GARLH4 left in AIP2 (n = 3 mice). Therefore, 33% of LHFPL4/GARLH4 was associated with NL2 in mouse brain homogenates.
One-way ANOVA followed by Dunnett's multiple comparisons test; ***$p < 0.001$ compared with the input. Data are mean ± SEM. See also Figure S1 and Table S1.

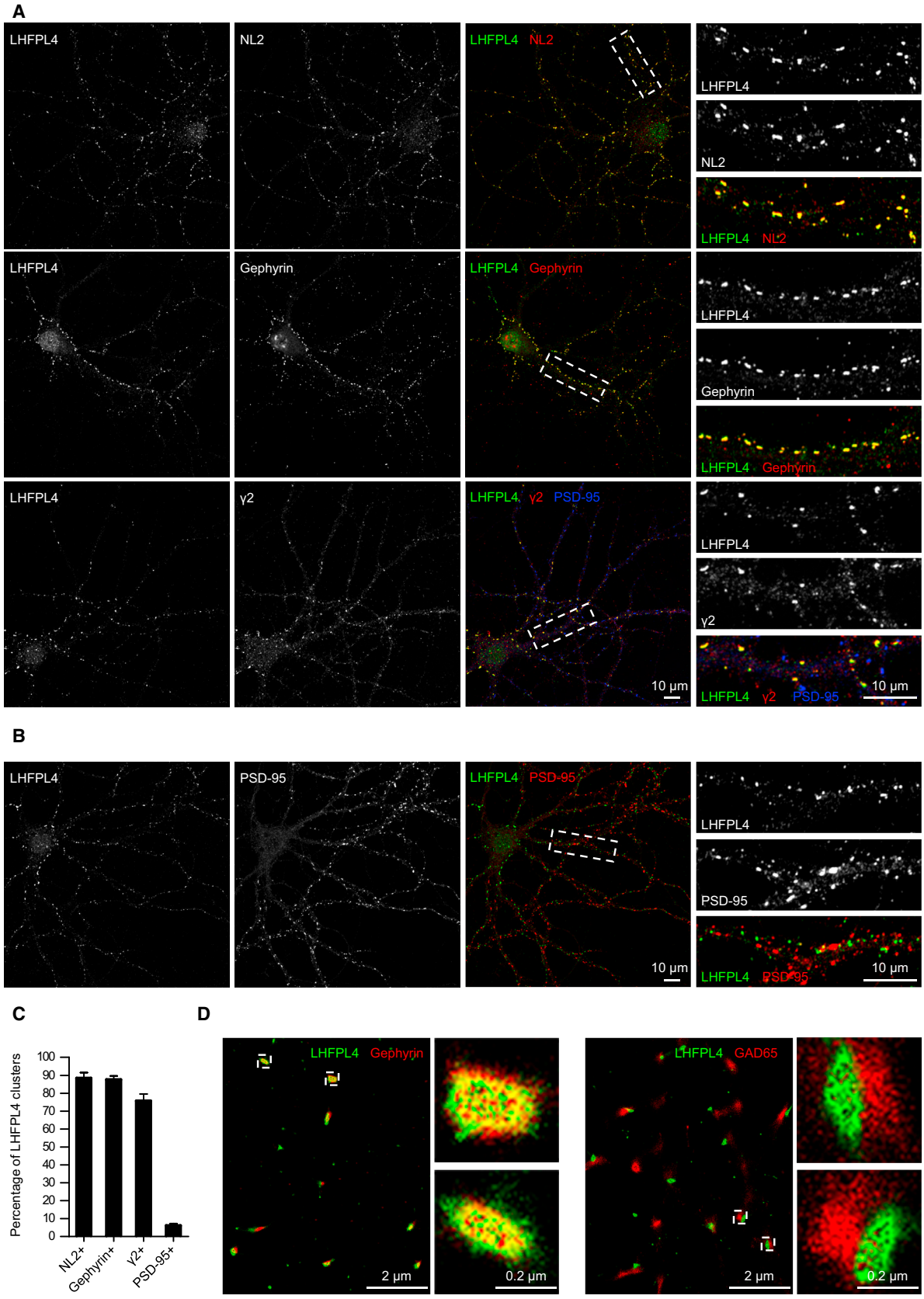

(legend on next page)

expressing short hairpin RNA (shRNA) that was able to knock down LHFPL4/GARLH4 (Figure S2D). Quantitative analysis of the co-immunostaining results showed that the majority of LHFPL4/GARLH4 puncta co-localized with clusters of inhibitory postsynaptic proteins, including NL2, gephyrin, and the $GABA_AR$ γ2 subunit (Figures 2A and 2C). In contrast, LHFPL4/GARLH4 puncta hardly co-localized with the excitatory postsynaptic scaffold protein PSD-95 (Figures 2B and 2C). Further investigation using a two-color super-resolution localization microscope showed that LHFPL4/GARLH4 puncta substantially overlapped with the postsynaptic gephyrin puncta but not with the presynaptic glutamic acid decarboxylase GAD65 puncta (Figure 2D). Thus, these data indicate that endogenous LHFPL4/GARLH4 is specifically enriched at inhibitory postsynaptic sites.

Knockdown of LHFPL4/GARLH4 Reduces the Number of Inhibitory Synapses in Cultured Hippocampal Neurons

We then addressed whether LHFPL4/GARLH4 was involved in inhibitory synapse formation by disrupting LHFPL4/GARLH4 expression using shRNA-mediated knockdown in primary cultured neurons. Two shRNAs against LHFPL4/GARLH4, sh-LHFPL4#1 and sh-LHFPL4#2, reduced both the exogenous expression of LHFPL4/GARLH4 in HEK293T cells and the endogenous expression of LHFPL4/GARLH4 in cultured neurons (Figure S2). Neurons with LHFPL4/GARLH4 knockdown by either sh-LHFPL4#1 or sh-LHFPL4#2 displayed a dramatic decrease in the number of NL2 and $GABA_AR$ γ2 clusters compared with neurons infected with AAV expressing the control shRNA (sh-Con) (Figures S3A and S3B). Co-expression of a shRNA-resistant Venus-tagged LHFPL4/GARLH4 mutant (Venus-LHFPL4*) was able to fully rescue the reduction in NL2 and $GABA_AR$ γ2 clusters caused by sh-LHFPL4#1 (Figures S2A, S3A, and S3B). In addition, knockdown of LHFPL4/GARLH4 also reduced the density of inhibitory synapses defined as vesicular GABA transporter (VGAT)-positive gephyrin clusters in neurons, which was then fully rescued by co-expression of Venus-LHFPL4* (Figure S3C). In contrast, knockdown of LHFPL4/GARLH4 did not affect the density of excitatory synapses defined as vesicular glutamate transporter 1 (VGLUT1)-positive PSD-95 clusters (Figure S3D). These data indicate that LHFPL4/GARLH4 selectively regulates inhibitory synapse formation in cultured neurons.

LHFPL4/GARLH4 KO Mice Die Prematurely

To further explore the role of LHFPL4/GARLH4 *in vivo*, we generated LHFPL4/GARLH4 KO mice using CRISPR-Cas9 technology (Figure 3A). Five independent *Lhfpl4/Garlh4* mutant mouse lines were obtained, among which the homozygous mutant mice in mouse lines 1, 2, and 3 survived to adulthood and were fertile, whereas the homozygous mutant mice in mouse lines 4 and 5 died prematurely (Table 1). Among the three viable mouse lines, although the originally proposed translation start codon would suggest that no LHFPL4/GARLH4 protein would be expressed with these three *Lhfpl4/Garlh4* mutations (Table S2, frame 1), an additional weak protein band migrating at a lower molecular weight than the WT LHFPL4/GARLH4 protein band was detected in the homozygous mutant mice brains (Figure S4A). This band may correspond to an N-terminal truncated LHFPL4/GARLH4 protein translated from the downstream start codon (Table S2, frame 2). Thus, the homozygous *Lhfpl4/Garlh4* mutant mice in these three viable mouse lines were incomplete LHFPL4/GARLH4 KO mice; the small amount of N-terminal truncated LHFPL4/GARLH4 protein in these mice may have been able to compensate for LHFPL4/GARLH4 function to certain degree and been sufficient for the mice to survive to adulthood. Neither of the two mouse lines in which the homozygous mutant mice died prematurely expressed any residual LHFPL4/GARLH4 protein (Figures 3B–3D; Figures S4A and S4B), indicating that they were complete LHFPL4/GARLH4 KO mice.

Lhfpl4/Garlh4$^{+/-}$ (mouse line 4 with a 7-bp deletion) breeding pairs produced offsprings with *Lhfpl4/Garlh4*$^{+/+}$, *Lhfpl4/Garlh4*$^{+/-}$, and *Lhfpl4/Garlh4*$^{-/-}$ genotypes in a 1:2:1 Mendelian ratio, suggesting that ablation of the LHFPL4/GARLH4 protein during embryogenesis is not lethal. Western blots using both anti-LHFPL4/GARLH4 antibodies determined that the LHFPL4/GARLH4 protein was undetectable in *Lhfpl4/Garlh4*$^{-/-}$ mouse brains (Figures 3C and 3D; Figures S4A and S4B), confirming the complete ablation of LHFPL4/GARLH4 in *Lhfpl4/Garlh4*$^{-/-}$ mice. There was no observable difference in the appearance or behavior of *Lhfpl4/Garlh4*$^{-/-}$ mice compared with *Lhfpl4/Garlh4*$^{+/+}$ and *Lhfpl4/Garlh4*$^{+/-}$ littermates at birth. However, all *Lhfpl4/Garlh4*$^{-/-}$ mice died prematurely, with a median survival time of 25 days (Figure 3E). The body weights of *Lhfpl4/Garlh4*$^{-/-}$ mice gradually increased until post-natal day 15 and then gradually decreased (Figure 3F). From post-natal day 11, the body weights of *Lhfpl4/Garlh4*$^{-/-}$ mice were found to be obviously less than those of *Lhfpl4/Garlh4*$^{+/+}$ and *Lhfpl4/Garlh4*$^{+/-}$ mice (Figure 3F). Around post-natal day 24, *Lhfpl4/Garlh4*$^{-/-}$ mice were much smaller in size (~50% reduction in body weight) than their WT littermates (Figure 3G). These results demonstrate that LHFPL4/GARLH4 is essential for postnatal survival.

LHFPL4/GARLH4 Is Highly Enriched in the Cerebellar Granular Layer and Regulates Inhibitory Synapse Formation *In Vivo*

Next, the expression profile of LHFPL4/GARLH4 in the mouse brain was investigated by western blot analysis. We dissected

Figure 2. Endogenous LHFPL4/GARLH4 Localizes to Inhibitory Postsynaptic Sites

(A and B) Cultured rat hippocampal neurons were immunostained for LHFPL4/GARLH4 using LHFPL4 Ab#1 and NL2 (A, top), gephyrin (A, center), $GABA_AR$ γ2 (A, bottom) or PSD-95 (B) at 16 days *in vitro* (DIV). LHFPL4/GARLH4 puncta co-localized with clusters of NL2, gephyrin, and $GABA_AR$ γ2 at inhibitory synapses but did not co-localize with PSD-95 at excitatory synapses. Scale bars represent 10 μm.

(C) Quantification of the percentage of LHFPL4/GARLH4 clusters co-localized with NL2, gephyrin, $GABA_AR$ γ2, and PSD95 clusters based on double labeling. One-way ANOVA, $p < 0.0001$, $n = 6–11$ cells. Data are mean ± SEM.

(D) Super-resolution images of cultured hippocampal neurons co-immunostained for LHFPL4/GARLH4 and gephyrin or GAD65. Scale bars represent 2 μm or 0.2 μm, as indicated.

See also Figures S2 and S3.

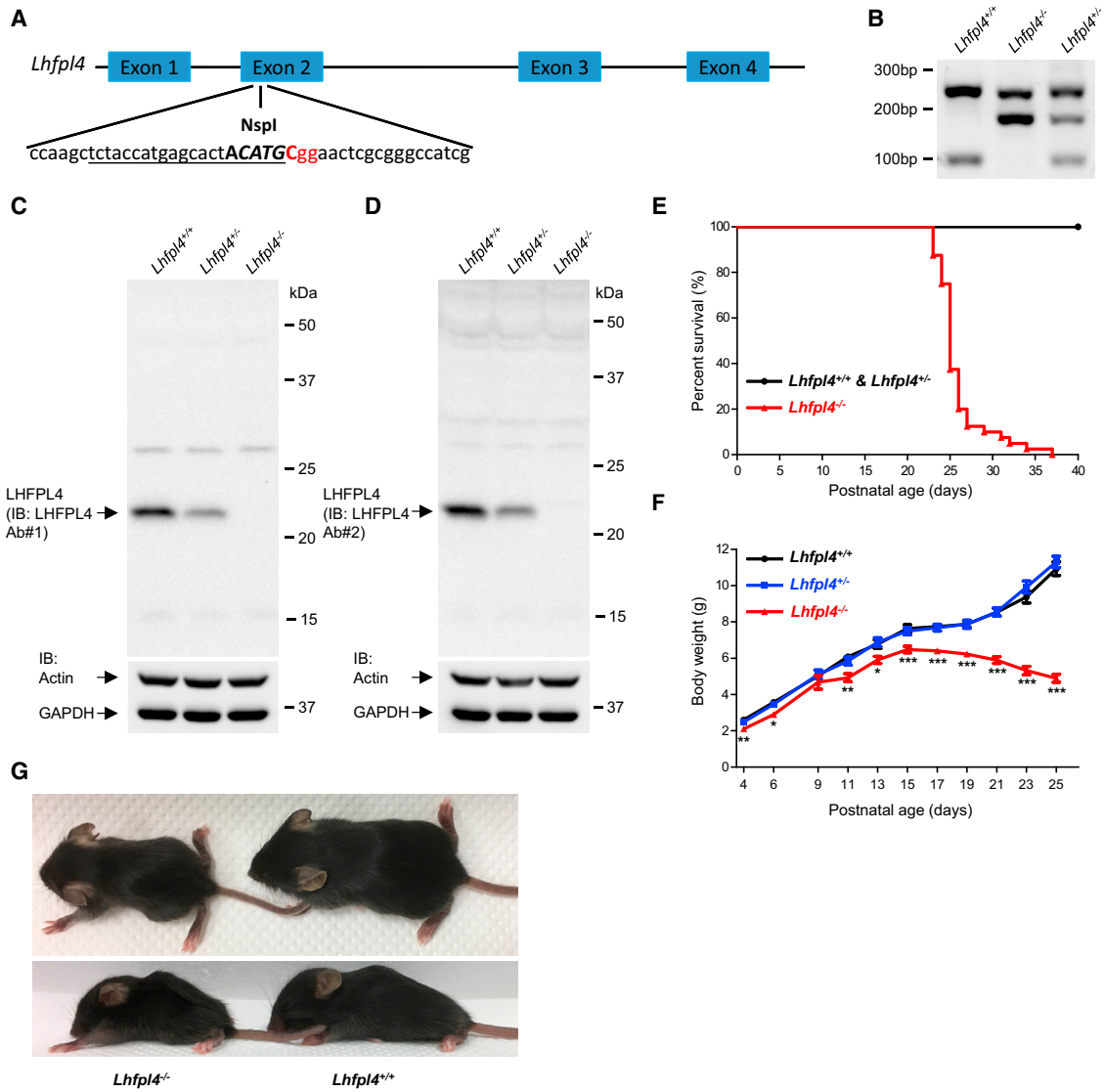

Figure 3. *Lhfpl4/Garlh4*$^{-/-}$ Mice Die Prematurely

(A) Schematic diagram of the Cas9/single guide RNA (sgRNA) targeting site in exon 2 of the *Lhfpl4/Garlh4* gene. The underlined sequence was targeted by sgRNA, and the red sequence is the protospacer-adjacent motif (PAM). The bold and capitalized sequence is the NspI restriction enzyme site used for the founder screening.

(B) Genotyping analysis of the mice in mouse line 4. The specific PCR products for the *Lhfpl4/Garlh4* WT and KO allele were 100 bp and 179 bp, respectively. A common band of 246 bp was produced by both WT and KO alleles.

(C and D) western blot analysis with LHFPL4 Ab#1 (C) and LHFPL4 Ab#2 (D) showed the absence of the LHFPL4/GARLH4 protein in brain homogenates from *Lhfpl4/Garlh4*$^{-/-}$ mice.

(E) Kaplan-Meier survival curves of *Lhfpl4/Garlh4*$^{+/+}$ (n = 37), *Lhfpl4/Garlh4*$^{+/-}$ (n = 75), and *Lhfpl4/Garlh4*$^{-/-}$ (n = 40) mice. The median survival time of *Lhfpl4/Garlh4*$^{-/-}$ mice was 25 days. Log rank (Mantel-Cox) test, $p < 0.0001$.

(F) The body weights of *Lhfpl4/Garlh4*$^{-/-}$ mice were obviously less than those of WT mice starting from post-natal day 11. No significant difference was detected between *Lhfpl4/Garlh4*$^{+/+}$ and *Lhfpl4/Garlh4*$^{+/-}$ mice. One-way ANOVA (n > 12 mice) followed by Dunnett's multiple comparisons test. Data are mean ± SEM; *$p < 0.05$, **$p < 0.01$, and ***$p < 0.001$ compared with WT mice.

(G) *Lhfpl4/Garlh4*$^{-/-}$ mice were much smaller in size than *Lhfpl4/Garlh4*$^{+/+}$ littermates at post-natal day 24.

the mouse brain into seven sub-regions, including the cortex, cerebellum, hippocampus, midbrain, olfactory bulb, pons plus medulla, as well as the rest of the brain. LHFPL4/GARLH4 and NL2 proteins were detected in all seven brain sub-regions (Figure 4A). We then performed immunohistochemical analysis to examine the localization pattern of LHFPL4/GARLH4 in the mouse brain. A strong specific signal of LHFPL4/GARLH4 was observed in the cerebellar granular layer (Figure 4B). LHFPL4/GARLH4 immunoreactivity with a punctate pattern was also observed in the cerebellar molecular layer (Figure 4B). In both

Table 1. Information Regarding the Five Lines of *Lhfpl4/Garlh4* Mutant Mice Generated by CRISPR-Cas9

		Homozygous Mice	
Mouse Line	Mutation Type	Viability and Fertility	LHFPL4/GARLH4 KO Efficiency
Line 1	14-bp deletion	survive to adulthood and are fertile	incomplete LHFPL4/GARLH4 KO
Line 2	8-bp deletion		
Line 3	1-bp insertion		
Line 4	7-bp deletion	die prematurely	complete LHFPL4/GARLH4 KO
Line 5	19-bp deletion		

Detailed information regarding the predicted protein sequence for each *Lhfpl4/Garlh4* mutant allele is provided in Table S2. Western blot analysis of whole-brain homogenates is provided in Figures S4A and S4B.

the cerebellar molecular layer and granular layer, LHFPL4/GARLH4 clusters co-localized with gephyrin at inhibitory synaptic sites (Figure 4C). LHFPL4/GARLH4 clusters also co-localized with gephyrin in the cortex and hippocampus (Figures S4C and S4D).

Strikingly, we observed a complete absence of the NL2 immunoreactivity in the cerebellar granular layer of *Lhfpl4/Garlh4*$^{-/-}$ mice compared with WT mice (Figure 4D). Interestingly, it seemed like NL2 immunoreactivity was not changed in the cerebellar molecular layer of *Lhfpl4/Garlh4*$^{-/-}$ mice (Figure 4D). We then performed quantitative immunohistochemical analysis of NL2 as well as other synaptic proteins on cerebellum cryosections from *Lhfpl4/Garlh4*$^{+/+}$, *Lhfpl4/Garlh4*$^{+/-}$, and *Lhfpl4/Garlh4*$^{-/-}$ mice. Notably, both the NL2 and $GABA_AR$ $\gamma2$ cluster area were dramatically smaller in the cerebellar granular layer of *Lhfpl4/Garlh4*$^{-/-}$ mice than in that of WT mice, and a significant reduction was also observed in the cerebellar granular layer of *Lhfpl4/Garlh4*$^{+/-}$ mice (Figure 5). *Lhfpl4/Garlh4*$^{-/-}$ mice also exhibited a smaller gephyrin cluster area than WT mice in the cerebellar granular layer (Figure 5A) but no difference in the NL2, $GABA_AR$ $\gamma2$, or gephyrin cluster area in the cerebellar molecular layer (Figure 5). We also examined excitatory postsynaptic receptor GluA2 (Figure 5B), the excitatory presynaptic marker VGLUT1, and the inhibitory presynaptic marker VGAT (Figure S5A), but no obvious change was observed in the cerebellum of *Lhfpl4/Garlh4*$^{-/-}$ mice. These data indicate that LHFPL4/GARLH4 plays a vital role in inhibitory synapse development *in vivo* by being involved in the clustering of inhibitory postsynaptic proteins.

LHFPL4/GARLH4 and NL2 Regulate Each Other's Protein Levels in the Cerebellum

We next examined whether LHFPL4/GARLH4 could regulate the protein levels of different inhibitory postsynaptic proteins, including NL2, $GABA_ARs$, and gephyrin, in the cerebellum of *Lhfpl4/Garlh4*$^{-/-}$ mice by western blot analysis. We detected an approximately 30% reduction in NL2 protein expression in *Lhfpl4/Garlh4*$^{-/-}$ mice compared with *Lhfpl4/Garlh4*$^{+/+}$ mice and a slight but significant reduction in NL2 protein in *Lhfpl4/Garlh4*$^{+/-}$ mice (Figure 6A). Similarly, an approximately 30% reduction in NL2 protein was also detected in the cortex and hippocampus of *Lhfpl4/Garlh4*$^{-/-}$ mice (Figure S6). An approximately 10% reduction in NL2 protein was detected in the midbrain of *Lhfpl4/Garlh4*$^{-/-}$ mice, but no significant difference was detected in the olfactory bulb, pons plus medulla, or the rest of the brain (Figure S6). Ablation of LHFPL4/GARLH4 had no effect on the protein expression of NL1, NL3, or the $GABA_AR$ $\alpha1$ or $\gamma2$ subunits (Figure 6A; Figure S6).

We also investigated whether NL2 could regulate the LHFPL4/GARLH4 protein level in the cerebellum. The cerebellum of NL2 KO mice contained significantly less LHFPL4/GARLH4 protein than the cerebellum of WT mice (Figure 6B). In contrast, ablation of both NL1 and NL3 did not affect LHFPL4/GARLH4 expression in the cerebellum of NL1/3 double KO mice (Figure 6B). We did not detect any significant difference in LHFPL4/GARLH4 expression in brain sub-regions other than the cerebellum from WT, NL2 KO, and NL1/3 double KO mice (Figure S7A). In addition, immunohistochemical analysis revealed that the LHFPL4/GARLH4 cluster area as well as the $GABA_AR$ $\gamma2$ cluster area were dramatically smaller in both the cerebellar granular layer and molecular layer of NL2 KO mice than in those of WT mice (Figures 6C and 6D). Ablation of NL2 moderately reduced the VGAT cluster area in the cerebellar molecular layer, but no obvious change was detected for excitatory presynaptic VGLUT1 clusters (Figure S5B). Taken together, these results demonstrate that LHFPL4/GARLH4 and NL2 regulate each other's protein levels in the cerebellum and that NL2 is required for the synaptic clustering of LHFPL4/GARLH4 in the cerebellum.

LHFPL4/GARLH4 KO Mice Exhibit Motor Behavioral Deficits

To further investigate whether impairment of inhibitory synapse formation in the cerebellum could result in behavioral deficits in *Lhfpl4/Garlh4*$^{-/-}$ mice, we examined cerebellum-related motor behaviors. When characterizing the phenotypes of *Lhfpl4/Garlh4*$^{-/-}$ mice, we noted abnormal limb clasping and altered gait. All *Lhfpl4/Garlh4*$^{-/-}$ mice displayed abnormal limb clasping when suspended by the tail that contrasted with the normal splaying behavior observed in *Lhfpl4/Garlh4*$^{+/+}$ and *Lhfpl4/Garlh4*$^{+/-}$ mice (Figure 7A). *Lhfpl4/Garlh4*$^{-/-}$ mice also had gait abnormalities, characterized by a markedly shorter stride length and a slightly smaller hindpaw base width compared with WT mice (Figure 7B). In addition, the fine motor coordination and hindlimb balance of the mice were assessed using the beam-walking test. *Lhfpl4/Garlh4*$^{-/-}$ mice showed poor performance on the beam, as they took significantly longer to cross the beam and exhibited more hindlimb foot slips during crossing than *Lhfpl4/Garlh4*$^{+/+}$ and *Lhfpl4/Garlh4*$^{+/-}$ mice (Figure 7C; Video S1). Besides examining the above cerebellum-related motor behaviors, we also investigated the effect of LHFPL4/GARLH4 deficiency on PTZ-induced seizure susceptibility in mice (PTZ is a $GABA_AR$ antagonist). The latency to both the first behavioral seizure and maximal tonic seizure in *Lhfpl4/Garlh4*$^{-/-}$ mice was significantly shorter than in *Lhfpl4/Garlh4*$^{+/+}$ and *Lhfpl4/Garlh4*$^{+/-}$ mice, and the latency to both seizure stages in *Lhfpl4/Garlh4*$^{+/-}$ mice was also significantly shorter than in *Lhfpl4/Garlh4*$^{+/+}$ mice (Figure S7B). Together, these results suggest that deletion of LHFPL4/GARLH4 increases seizure susceptibility and leads to motor impairment as a result of reduction in inhibitory synapse number.

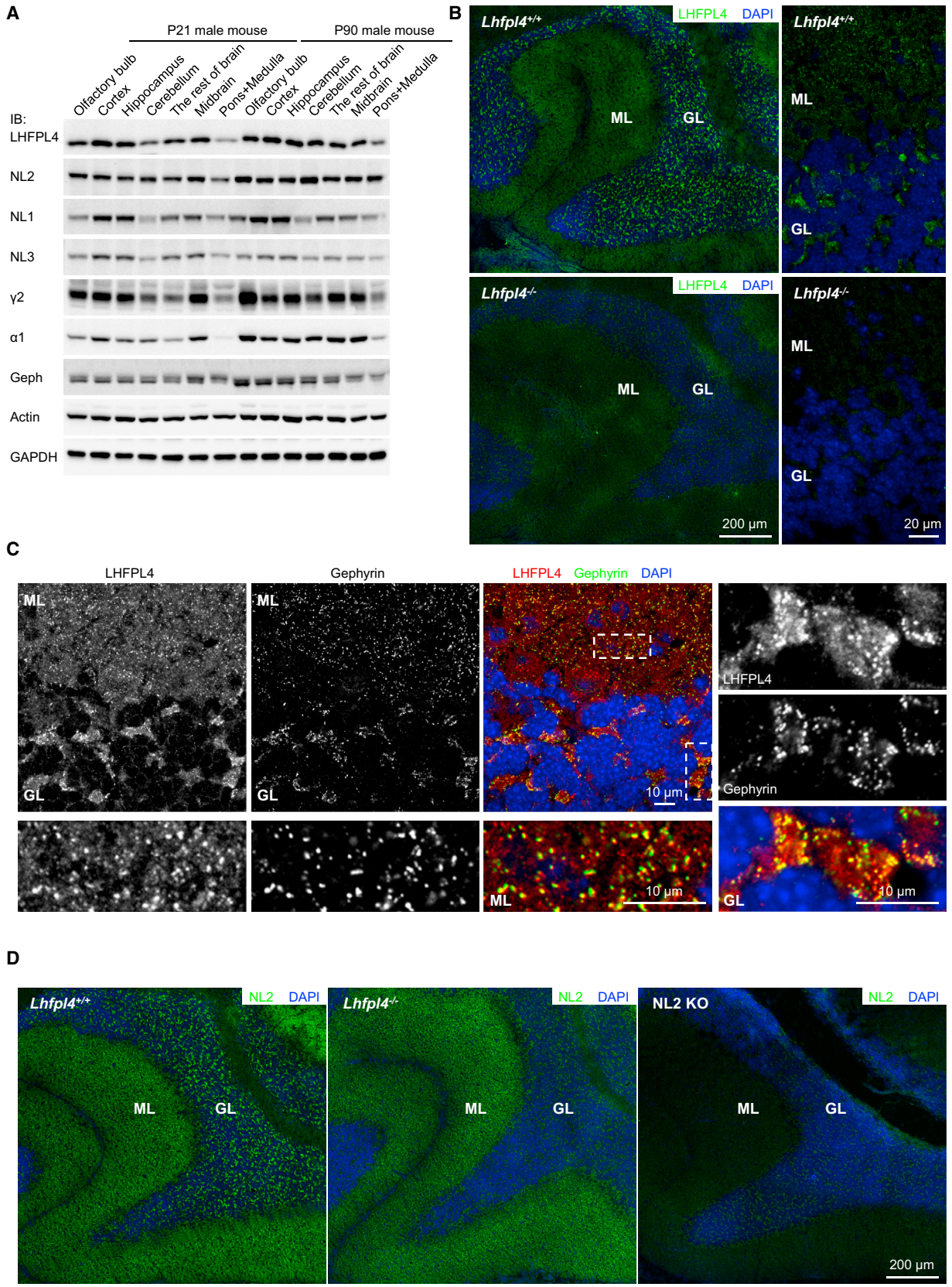

(legend on next page)

DISCUSSION

The molecular mechanisms underlying synaptogenesis are not completely elucidated. This is especially true for the inhibitory synapses; the meager list of inhibitory PSD proteins has impeded the understanding of the molecular mechanisms underlying inhibitory postsynaptic regulation and related brain disorders. In this study, we identified LHFPL4/GARLH4 as a major NL2 binding partner using immunoprecipitation coupled with mass spectrometry analysis. By conducting quantitative co-immunoprecipitation experiments, we found that significant proportions (approximately 30%) of LHFPL4/GARLH4 and NL2 are associated with each other in the mouse brain (Figures 1E–1H). The tight association between LHFPL4/GARLH4 and NL2 is important for their mutual regulation of the protein level and synaptic clustering because loss of one led to significant reductions of the other protein's level and synaptic clustering (Figures 5A and 6). LHFPL4/GARLH4 is specifically enriched at inhibitory synapses but not at excitatory synapses, and super-resolution imaging further revealed postsynaptic localization of LHFPL4/GARLH4 (Figure 2). The functional specificity of LHFPL4/GARLH4 at inhibitory synapses, as suggested by the subcellular localization, is also supported by the selective loss of the $GABA_AR$ γ2 clusters as well as the NL2 and gephyrin clusters, but not the excitatory synaptic protein clusters, in the cerebellar granular layer of *Lhfpl4/Garlh4*$^{-/-}$ mice (Figure 5). Interestingly, ablation of LHFPL4/GARLH4 did not affect the presynaptic VGAT clusters in the cerebellum (Figure S5A). These results suggest a rather specific role for LHFPL4/GARLH4 at postsynaptic sites, and it may not regulate inhibitory synapse formation *trans*-synaptically. Thus, LHFPL4/GARLH4 is likely to function as an organizing protein at the inhibitory postsynaptic site and act in concert with NL2 to recruit or stabilize $GABA_ARs$.

Different $GABA_AR$ subtypes display different regional brain distributions, subcellular localizations, and functional properties (Olsen and Sieghart, 2008). Interestingly, we observed a dramatic decrease in the number of NL2 and $GABA_AR$ γ2 puncta in the cerebellar granular layer of *Lhfpl4/Garlh4*$^{-/-}$ mice but no change in the cerebellar molecular layer (Figures 4D and 5). This could be due to the different types of postsynaptic neurons expressing LHFPL4/GARLH4 in the granular and molecular layers of the cerebellum. In the granular layer, GABAergic synapses are mainly formed onto excitatory neurons (Sassoè-Pognetto and Patrizi, 2013). This is in contrast to the molecular layer, where GABAergic synapses are mainly formed onto inhibitory neurons. As reported by Davenport et al. (2017), LHFPL4/GARLH4 is essential for $GABA_AR$ clustering only in excitatory neurons. Thus, LHFPL4/GARLH4 may regulate inhibitory synapse formation in an excitatory neuron-specific manner in the brain. However, given the complexity of inhibitory interneurons (Kepecs and Fishell, 2014), it remains to be determined whether all or only a subset of the interneurons are resistant to LHFPL4/GARLH4 deletion. In contrast to LHFPL4/GARLH4, the adhesion molecule IgSF9b was found to be abundantly expressed in GABAergic interneurons and to preferentially promote inhibitory synapse formation onto inhibitory interneurons by coupling to NL2 via S-SCAM (Woo et al., 2013). These findings suggest that NL2 works in parallel with different proteins to drive neuron type-specific inhibitory synapse development.

We found that approximately 30% of LHFPL4/GARLH4 and NL2 are associated with each other in the mouse brain (Figures 1E–1H) and that loss of one leads to a significant reduction of the other protein's level only in specific brain sub-regions (Figures 6A and 6B; Figures S6 and S7A). Together with the above-described granular layer-specific loss of NL2 and $GABA_AR$ γ2 clusters in the cerebellum of *Lhfpl4/Garlh4*$^{-/-}$ mice, these data suggest that the association between LHFPL4/GARLH4 and NL2 may be brain region-specific and neuron type-specific. It is possible that LHFPL4/GARLH4 works in concert with an array of synaptogenic adhesion molecules to drive inhibitory synapse development in different brain regions and neurons, whereas NL2 also works in concert with other LHFPL4/GARLH4-like proteins. Therefore, further studies designed to identify corresponding organizing proteins for a defined $GABA_AR$ subtype expressed in specific neurons or in a specific brain region could provide a more comprehensive picture of inhibitory synapse organization in the brain.

Accompanying the impairment of inhibitory synapse formation in the cerebellum, we observed prominent motor behavioral deficits in *Lhfpl4/Garlh4*$^{-/-}$ mice. In addition, LHFPL4/GARLH4 deficiency leads to greater seizure susceptibility, suggesting an increase in neuronal excitability. These results strongly support an essential role for LHFPL4/GARLH4 in brain functions. Furthermore, the premature death of *Lhfpl4/Garlh4*$^{-/-}$ mice indicates that LHFPL4/GARLH4 is dispensable for embryonic development but essential for postnatal survival. However, a detailed examination is required to determine the reason for the death of the *Lhfpl4/Garlh4*$^{-/-}$ mice. More comprehensive and systematic analyses of the behavior and synapse development in neuron-specific or brain region-specific LHFPL4/GARLH4 KO mice would provide insight into the precise role of LHFPL4/GARLH4 in brain functions.

Mice lacking NL2 also exhibit deficits in synaptic $GABA_AR$ clusters as well as increased neuronal excitability (Babaev

Figure 4. LHFPL4/GARLH4 Is Highly Enriched in the Cerebellar Granular Layer and Regulates the Synaptic Clustering of NL2

(A) Widespread distribution of the LHFPL4/GARLH4 protein in different mouse brain sub-regions at post-natal day 21 (P21) and P90.

(B) Immunostaining of the cerebellum with LHFPL4 Ab#2. The nuclei were labeled by DAPI. Strong LHFPL4/GARLH4 immunoreactivity was found in the cerebellar granular layer of WT mice. Specific immunoreactivity with a punctate pattern was also observed in the cerebellar molecular layer. *Lhfpl4/Garlh4*$^{-/-}$ mice showed only a background signal.

(C) Immunofluorescence for LHFPL4/GARLH4 and gephyrin in the cerebellum. LHFPL4/GARLH4 formed clusters in the molecular layer as well as in the granular layer, and these clusters co-localized with gephyrin.

(D) Immunofluorescence for NL2 in the cerebellum of *Lhfpl4/Garlh4*$^{+/+}$, *Lhfpl4/Garlh4*$^{-/-}$ and NL2 KO mice. *Lhfpl4/Garlh4*$^{-/-}$ mice exhibited a complete absence of NL2 immunoreactivity in the granular layer compared with WT mice. Lack of NL2 immunoreactivity in the NL2 KO mice confirmed the specificity of the antibody. GL, granular layer; ML, molecular layer. Scale bars represent 200 μm (B, left, and D), 20 μm (B, right), and 10 μm (C). See also Figure S4.

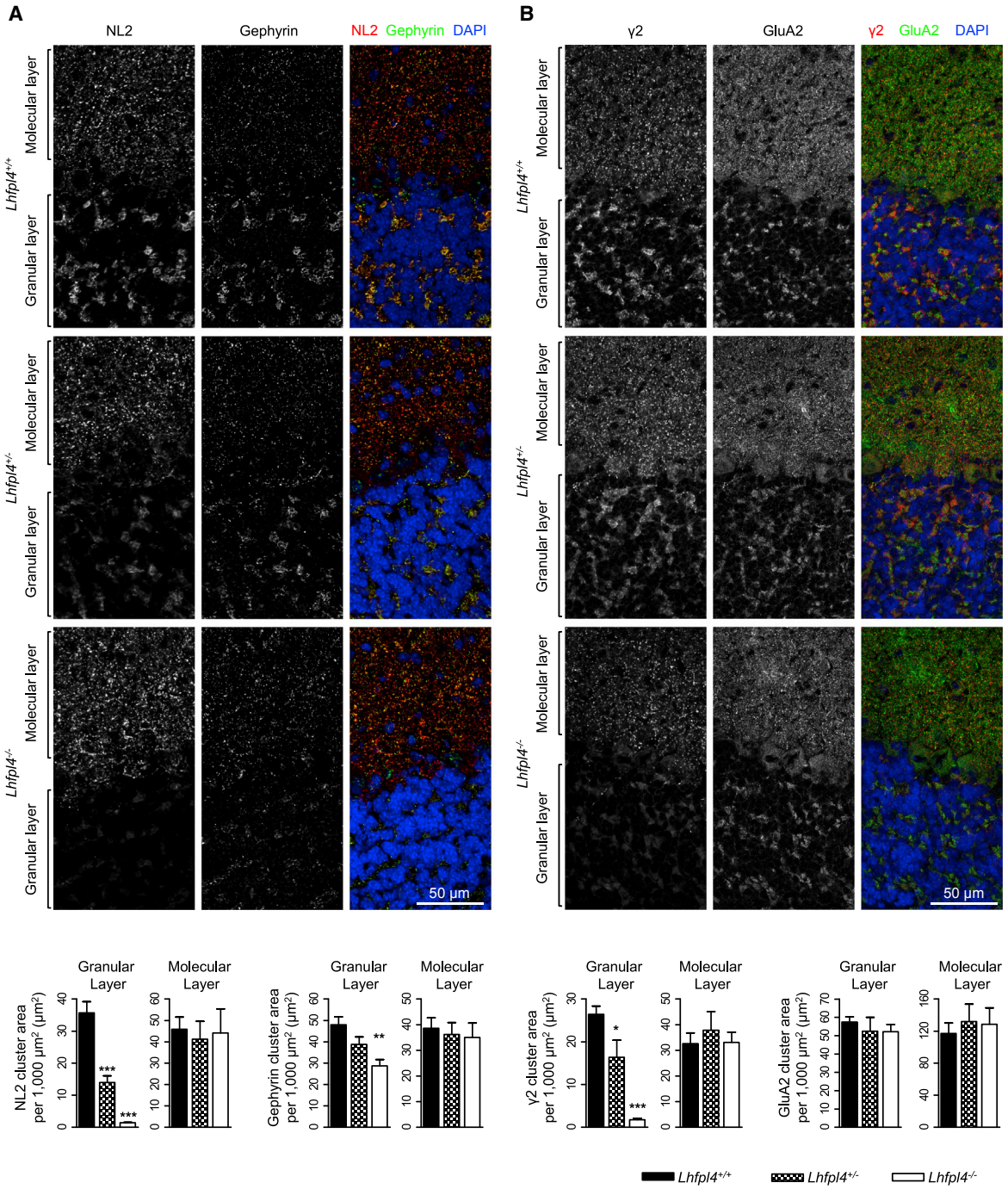

Figure 5. *Lhfpl4/Garlh4*$^{-/-}$ Mice Have Reduced Inhibitory Synapse Density in the Granular Layer of the Cerebellum

Immunohistochemical analysis of clusters of postsynaptic proteins in the cerebellum from *Lhfpl4/Garlh4*$^{+/+}$, *Lhfpl4/Garlh4*$^{+/-}$, and *Lhfpl4/Garlh4*$^{-/-}$ mice. The nuclei were labeled by DAPI. The area (μm^2 per 1,000 μm^2) of clustered NL2 (A) and $GABA_AR$ γ2 (B) showed a marked reduction in the cerebellar granular layer of *Lhfpl4/Garlh4*$^{-/-}$ mice compared with WT mice. A significant reduction in the NL2 and $GABA_AR$ γ2 cluster area was also observed in the cerebellar granular layer of *Lhfpl4/Garlh4*$^{+/-}$ mice. The gephyrin cluster area (A) was decreased in the cerebellar granular layer of *Lhfpl4/Garlh4*$^{-/-}$ mice. The area of clustered NL2, $GABA_AR$ γ2, and gephyrin remained unchanged in the cerebellar molecular layer of *Lhfpl4/Garlh4*$^{-/-}$ mice. The GluA2 cluster area (B) was not altered.

One-way ANOVA, n = 5–6 mice for each genotype. $p < 0.0001$ and $p = 0.9353$ for the NL2 cluster area, $p = 0.0041$ and $p = 0.8581$ for the gephyrin cluster area, $p < 0.0001$ and $p = 0.7577$ for the $GABA_AR$ γ2 cluster area, and $p = 0.7374$ and $p = 0.8374$ for the GluA2 cluster area in the granular layer and molecular layer, respectively. *$p < 0.05$, **$p < 0.01$, and ***$p < 0.001$ compared with WT mice by Dunnett's multiple comparisons test. Data are mean ± SEM. Scale bars represent 50 μm. See also Figure S5.

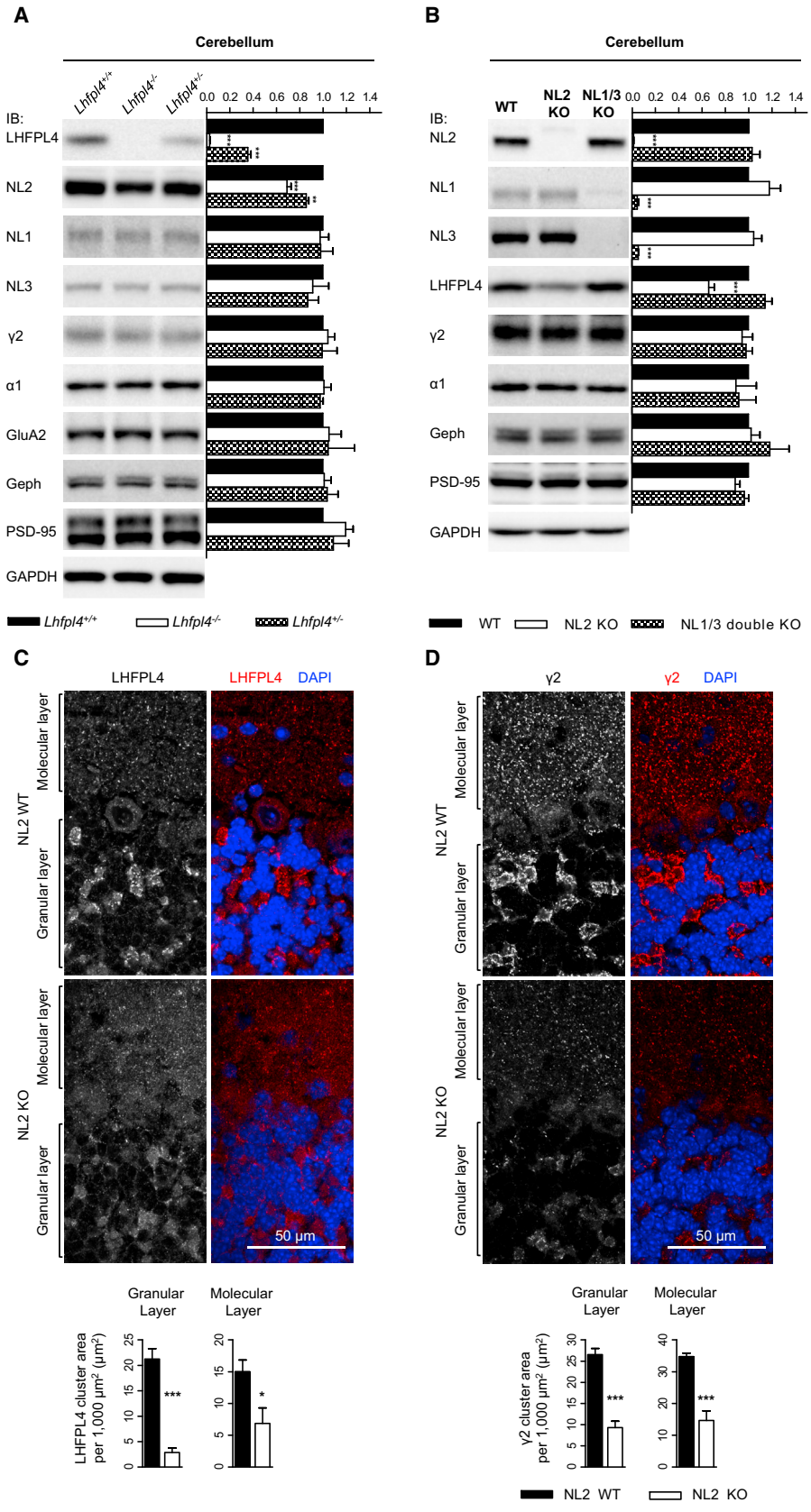

(legend on next page)

et al., 2016; Blundell et al., 2009; Hoon et al., 2009; Jedlicka et al., 2011; Poulopoulos et al., 2009). However, unlike LHFPL4/GARLH4 KO mice, NL2 KO mice are able to survive to adulthood with relatively subtle functional defects (Varoqueaux et al., 2006). This difference may be explained by the existence of other synaptogenic adhesion molecules, such as NL3 (Budreck and Scheiffele, 2007), NL4 (Hoon et al., 2011), Slitrk3 (Takahashi et al., 2012), Calsyntenin-3 (Pettem et al., 2013), and IgSF21 (Tanabe et al., 2017), which may control inhibitory synapse formation and compensate for the loss of NL2 at inhibitory synapses. Like NL2 KO mice, mice with ablation of NL3, NL4, Slitrk3, Calsyntenin-3, or IgSF21 also show no obvious deficits in survival (Jamain et al., 2008; Pettem et al., 2013; Takahashi et al., 2012; Tanabe et al., 2017; Varoqueaux et al., 2006), suggesting a redundancy of cell adhesion molecules in the regulation of inhibitory synapse formation. However, the retarded growth and markedly decreased lifespan in LHFPL4/GARLH4 KO mice suggest a more essential and indispensable role for LHFPL4/GARLH4 in the formation of inhibitory circuits. A similar functional importance of gephyrin and $GABA_AR$ $\gamma2$ is also demonstrated by a drastic reduction in the lifespan of gephyrin KO mice and $GABA_AR$ $\gamma2$ KO mice, respectively (Feng et al., 1998; Günther et al., 1995). $GABA_AR$ $\gamma2$ is the most abundant $GABA_AR$ subunit and exists in approximately 75% to 80% of $GABA_ARs$ in the CNS (Olsen and Sieghart, 2008), whereas gephyrin is the core scaffolding protein anchoring glycine receptors and $GABA_ARs$ in the inhibitory PSD (Tyagarajan and Fritschy, 2014). Thus, LHFPL4/GARLH4 may also serve as a core organizing protein for inhibitory synapse formation, and, as a result, its deficiency is detrimental to the survival of animals.

LHFPL4/GARLH4 has been reported to be associated with $GABA_ARs$ in two proteomics studies of inhibitory synapses (Heller et al., 2012; Nakamura et al., 2016). However, the function of LHFPL4/GARLH4 was not reported until recently, while our work was ongoing. Using mass spectrometry analysis, Yamasaki et al. (2017) identified LHFPL4/GARLH4 as part of the 720-kDa $GABA_AR$ complex and demonstrated that NL2 was also a part of this complex. It is reassuring that, although Yamasaki et al. (2017) and we started from different inhibitory PSD targets, $GABA_AR$ $\alpha1$ and NL2, respectively, we both demonstrated a crucial role for LHFPL4/GARLH4 in inhibitory synapse formation. Furthermore, our *in vivo* studies with *Lhfpl4/Garlh4*$^{-/-}$ mice revealed an essential role for LHFPL4/GARLH4 in brain functions and postnatal survival.

Davenport et al. (2017) recently reported a LHFPL4/GARLH4 KO mouse line that was viable until adulthood and fertile, in contrast to the premature death of LHFPL4/GARLH4 KO mice observed in our study. There are a number of potential explanations for this discrepancy. First, among the five independent lines of *Lhfpl4/Garlh4* mutant mice we obtained, three resulted in homozygous mutant mice that were also viable (Table 1). The viability of these mice was due to a small amount of N-terminal truncated LHFPL4/GARLH4 protein that was expressed in the homozygous mutant mice and was sufficient for the mice to survive to adulthood (Figure S4A). The LHFPL4/GARLH4 KO mice reported by Davenport et al. (2017) may have similarly expressed a small amount of N-terminal truncated LHFPL4/GARLH4 protein. Second, the discrepancy may be due to the different genetic backgrounds of the mouse lines. We used CRISPR-Cas9 technology to generate mutant mice and C57BL/6J mice for both embryo microinjection and backcrossing. The exact mouse line used by Davenport et al. (2017) was not stated, but they used a standard knockout technique that usually involves two different mouse lines for microinjection and backcrossing. Third, off-target mutations may have caused the premature death of our mice. This is, however, very unlikely. Five independent lines of *Lhfpl4/Garlh4* mutant mice were generated in our study. Only the homozygous mutant mice in the two lines with complete deletion of LHFPL4/GARLH4 died prematurely. The chance that a lethal off-target effect would only exist in the two LHFPL4/GARLH4 complete KO mouse lines but not in the three LHFPL4/GARLH4 incomplete KO mouse lines is extremely low.

Accumulating evidence has linked genes encoding inhibitory synapse-organizing proteins to brain disorders (Krueger-Burg et al., 2017). Thus, the assessment of LHFPL4/GARLH4 in brain disorders is important. Considering that LHFPL4/GARLH4 deletion in mice leads to motor behavioral deficits and increased seizure susceptibility (Figure 7; Figure S7B), study of the *Lhfpl4/Garlh4* gene in patients with epilepsy or other brain disorders characterized by motor behavioral deficits would be informative. Moreover, analysis of LHFPL4/GARLH4 protein expression or LHFPL4/GARLH4 puncta in post mortem brain samples from patients with these disorders is also desirable.

EXPERIMENTAL PROCEDURES

Animals

All experimental procedures involving animals were conducted in compliance with protocols approved by the Animal Ethics Committee at the Hong Kong University of Science and Technology (HKUST). Animals were maintained in a 12-hr light/dark cycle with free access to water and food. Sprague-Dawley rats (strain code 400) were obtained from Charles River Laboratories. B6 WT mice (C57BL/6J, stock no. 000664), NL1 KO mice (stock no. 008136), NL2 KO mice (stock no. 008139), and NL3 KO mice (stock no. 008394) were ordered from Jackson Laboratory. NL1/3 double KO mice were generated by cross-breeding NL1 KO mice with NL3 KO mice. LHFPL4/GARLH4 KO mice were generated using CRISPR-Cas9 technology. For the western blot analysis involving NL1/3 double KO mice, age-matched (same day of birth) and sex-matched WT mice and NL2 KO mice were used. LHFPL4/GARLH4 mice at post-natal days 17–21 and NL mice at post-natal days 24–45 were used for

Figure 6. LHFPL4/GARLH4 and NL2 Regulate Each Other's Protein Levels in the Cerebellum

(A) Expression levels of synaptic proteins in the cerebellum from *Lhfpl4/Garlh4*$^{+/+}$, *Lhfpl4/Garlh4*$^{-/-}$, and *Lhfpl4/Garlh4*$^{+/-}$ mice.

(B) Expression levels of synaptic proteins in the cerebellum from WT, NL2 KO, and NL1/3 double KO mice.

(C and D) Immunohistochemical analysis of clusters of LHFPL4/GARLH4 and $GABA_AR$ $\gamma2$ in the cerebellum from NL2 WT and KO mice. The nuclei were labeled by DAPI. The area (μm^2 per 1,000 μm^2) of clustered LHFPL4/GARLH4 (C) and $GABA_AR$ $\gamma2$ (D) showed a marked reduction in the cerebellar granular layer and molecular layer in NL2 KO mice compared with WT mice. Scale bars represent 50 μm.

n = 4 mice for each genotype; one-way ANOVA followed by Dunnett's multiple comparisons test in (A) and (B) and unpaired t test in (C) and (D). *$p < 0.05$, **$p < 0.01$, ***$p < 0.001$ compared with WT mice. Data are mean ± SEM. See also Figures S5–S7.

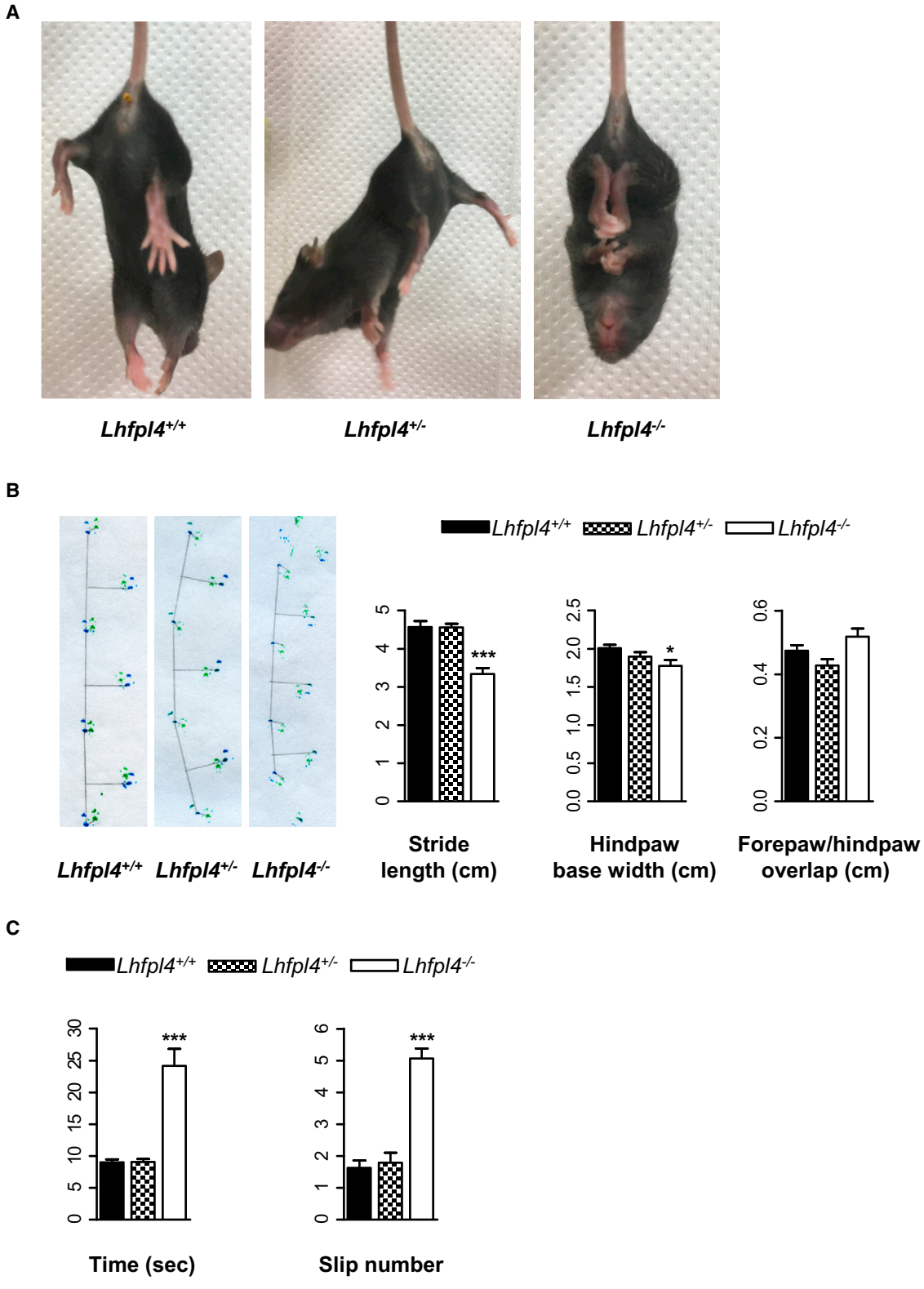

Figure 7. *Lhfpl4/Garlh4*$^{-/-}$ Mice Have Motor Behavioral Deficits

(A) All *Lhfpl4/Garlh4*$^{-/-}$ mice displayed abnormal limb clasping when suspended by the tail. *Lhfpl4/Garlh4*$^{+/+}$ and *Lhfpl4/Garlh4*$^{+/-}$ mice displayed normal splaying.

(legend continued on next page)

biochemical and histochemical studies. LHFPL4/GARLH4 mice at post-natal days 17–18 were used for behavior tests. Rat embryos at embryonic day 18 were used for the preparation of primary cultured neurons. Animals of either sex were used.

Quantification and Statistical Analysis

The immunoblots were visualized using the ChemiDoc Touch Imaging System (Bio-Rad), and protein band intensity was measured using Image Lab software (Bio-Rad). For the quantifications shown in Figures 6A, 6B, S4B, S6, and S7A, the chemiluminescence intensity of the protein was first normalized by that of GAPDH on the same membrane, and then the value of the WT mice was normalized to 1 for comparison. To measure the density or the area of synaptic clusters in cultured neurons and brain slices, compared images were thresholded using a constant threshold value in ImageJ. The threshold value was calculated as the mean of the manually selected threshold value, which was visually confirmed to select appropriate clusters. The length of dendrites in cultured neurons was measured using ImageJ with the NeuronJ plugin. The synapse density in cultured neurons was measured as the number of clusters per micrometer, and the synapse density in brain slices was measured as the cluster area (square micrometers) per 1,000 μm^2. Adobe Photoshop CS6 was used to adjust the brightness and contrast of the images and to choose the region of interest. The Mendelian segregation ratio was analyzed with χ^2 test in RStudio. GraphPad Prism 6 was used to perform all other statistical analyses and plot all data. The sample sizes were determined based on previous studies in the field. All reported values are mean ± SEM. The statistical analysis methods used are indicated in the figure legends. Asterisks indicate a significant difference (*$p < 0.05$, **$p < 0.01$, and ***$p < 0.001$).

SUPPLEMENTAL INFORMATION

Supplemental Information includes Supplemental Experimental Procedures, seven figures, two tables, and one video and can be found with this article online at https://doi.org/10.1016/j.celrep.2018.04.015.

ACKNOWLEDGMENTS

We thank Prof. Ning Li for advice regarding mass spectrometry, Wai Lin Tung and Shui Wa Yun for technical support, and Dr. Chuen Kam for critical reading of the manuscript. We also thank NanoBioImaging Ltd. for the super-resolution image analysis software. This work was supported in part by the Research Grants Council of the Hong Kong SAR, China (16146516, 16102914, 663613, N_HKUST625/15, HKUST10/CRF/12R, HKUST12/CRF/13G, C4011-14R, T13-607/12R, AoE/M-05/12, and AoE/M-604/16). S.D. acknowledges support from the Offices of Provost, VPRG, and Dean of Science, HKUST (VPRGO12SC02).

AUTHOR CONTRIBUTIONS

M.W. and J.X. designed the study, analyzed the data, and wrote the manuscript. M.W., H.-L.T., X.L., and J.H.C.L. conducted the experiments. S.D. developed the two-color super-resolution localization microscope and imaging technique. All authors contributed to discussions and commented on the manuscript.

DECLARATION OF INTERESTS

The authors declare no competing interests.

Received: November 2, 2017
Revised: February 26, 2018
Accepted: April 2, 2018
Published: May 8, 2018

REFERENCES

Babaev, O., Botta, P., Meyer, E., Müller, C., Ehrenreich, H., Brose, N., Lüthi, A., and Krueger-Burg, D. (2016). Neuroligin 2 deletion alters inhibitory synapse function and anxiety-associated neuronal activation in the amygdala. Neuropharmacology *100*, 56–65.

Blundell, J., Tabuchi, K., Bolliger, M.F., Blaiss, C.A., Brose, N., Liu, X., Südhof, T.C., and Powell, C.M. (2009). Increased anxiety-like behavior in mice lacking the inhibitory synapse cell adhesion molecule neuroligin 2. Genes Brain Behav. *8*, 114–126.

Budreck, E.C., and Scheiffele, P. (2007). Neuroligin-3 is a neuronal adhesion protein at GABAergic and glutamatergic synapses. Eur. J. Neurosci. *26*, 1738–1748.

Chih, B., Engelman, H., and Scheiffele, P. (2005). Control of excitatory and inhibitory synapse formation by neuroligins. Science *307*, 1324–1328.

Chubykin, A.A., Atasoy, D., Etherton, M.R., Brose, N., Kavalali, E.T., Gibson, J.R., and Südhof, T.C. (2007). Activity-dependent validation of excitatory versus inhibitory synapses by neuroligin-1 versus neuroligin-2. Neuron *54*, 919–931.

Davenport, E.C., Pendolino, V., Kontou, G., McGee, T.P., Sheehan, D.F., López-Doménech, G., Farrant, M., and Kittler, J.T. (2017). An Essential Role for the Tetraspanin LHFPL4 in the Cell-Type-Specific Targeting and Clustering of Synaptic $GABA_A$Receptors. Cell Rep. *21*, 70–83.

Feng, G., Tintrup, H., Kirsch, J., Nichol, M.C., Kuhse, J., Betz, H., and Sanes, J.R. (1998). Dual requirement for gephyrin in glycine receptor clustering and molybdoenzyme activity. Science *282*, 1321–1324.

Foss-Feig, J.H., Adkinson, B.D., Ji, J.L., Yang, G., Srihari, V.H., McPartland, J.C., Krystal, J.H., Murray, J.D., and Anticevic, A. (2017). Searching for Cross-Diagnostic Convergence: Neural Mechanisms Governing Excitation and Inhibition Balance in Schizophrenia and Autism Spectrum Disorders. Biol. Psychiatry *81*, 848–861.

Fritschy, J.M. (2008). Epilepsy, E/I Balance and GABA(A) Receptor Plasticity. Front. Mol. Neurosci. *1*, 5.

Gibson, J.R., Huber, K.M., and Südhof, T.C. (2009). Neuroligin-2 deletion selectively decreases inhibitory synaptic transmission originating from fast-spiking but not from somatostatin-positive interneurons. J. Neurosci. *29*, 13883–13897.

Graf, E.R., Zhang, X., Jin, S.X., Linhoff, M.W., and Craig, A.M. (2004). Neurexins induce differentiation of GABA and glutamate postsynaptic specializations via neuroligins. Cell *119*, 1013–1026.

Greger, I.H., Watson, J.F., and Cull-Candy, S.G. (2017). Structural and Functional Architecture of AMPA-Type Glutamate Receptors and Their Auxiliary Proteins. Neuron *94*, 713–730.

Günther, U., Benson, J., Benke, D., Fritschy, J.M., Reyes, G., Knoflach, F., Crestani, F., Aguzzi, A., Arigoni, M., Lang, Y., et al. (1995). Benzodiazepine-insensitive mice generated by targeted disruption of the gamma 2 subunit gene of gamma-aminobutyric acid type A receptors. Proc. Natl. Acad. Sci. USA *92*, 7749–7753.

(B) Representative footprint patterns and the quantification of step parameters. The stride length of *Lhfpl4/Garlh4*$^{-/-}$ mice (n = 8) was markedly shorter than that of WT mice (n = 10), whereas the hindpaw base width of *Lhfpl4/Garlh4*$^{-/-}$ mice was slightly smaller. There was no significant difference in forepaw/hindpaw overlap between *Lhfpl4/Garlh*$^{-/-}$ and *Lhfpl4/Garlh4*$^{+/+}$ mice. No significant difference was detected between *Lhfpl4/Garlh4*$^{+/+}$ and *Lhfpl4/Garlh4*$^{+/-}$ (n = 11) mice.
(C) Quantification of the time to cross the beam and the number of hindlimb foot slips in the beam-walking test. *Lhfpl4/Garlh4*$^{-/-}$ mice (n = 7) required longer to cross the beam and had more foot slips than *Lhfpl4/Garlh4*$^{+/+}$ (n = 10) and *Lhfpl4/Garlh4*$^{+/-}$ (n = 11) mice. No significant difference was detected between *Lhfpl4/Garlh4*$^{+/+}$ and *Lhfpl4/Garlh4*$^{+/-}$ mice.
One-way ANOVA followed by Dunnett's multiple comparisons test. Data are mean ± SEM; *$p < 0.05$ and ***$p < 0.001$ compared with WT mice. See also Figure S7 and Video S1.

Heller, E.A., Zhang, W., Selimi, F., Earnheart, J.C., Ślimak, M.A., Santos-Torres, J., Ibañez-Tallon, I., Aoki, C., Chait, B.T., and Heintz, N. (2012). The biochemical anatomy of cortical inhibitory synapses. PLoS ONE *7*, e39572.

Hoftman, G.D., Datta, D., and Lewis, D.A. (2017). Layer 3 Excitatory and Inhibitory Circuitry in the Prefrontal Cortex: Developmental Trajectories and Alterations in Schizophrenia. Biol. Psychiatry *81*, 862–873.

Hoon, M., Bauer, G., Fritschy, J.M., Moser, T., Falkenburger, B.H., and Varoqueaux, F. (2009). Neuroligin 2 controls the maturation of GABAergic synapses and information processing in the retina. J. Neurosci. *29*, 8039–8050.

Hoon, M., Soykan, T., Falkenburger, B., Hammer, M., Patrizi, A., Schmidt, K.F., Sassoè-Pognetto, M., Löwel, S., Moser, T., Taschenberger, H., et al. (2011). Neuroligin-4 is localized to glycinergic postsynapses and regulates inhibition in the retina. Proc. Natl. Acad. Sci. USA *108*, 3053–3058.

Jamain, S., Radyushkin, K., Hammerschmidt, K., Granon, S., Boretius, S., Varoqueaux, F., Ramanantsoa, N., Gallego, J., Ronnenberg, A., Winter, D., et al. (2008). Reduced social interaction and ultrasonic communication in a mouse model of monogenic heritable autism. Proc. Natl. Acad. Sci. USA *105*, 1710–1715.

Jedlicka, P., Hoon, M., Papadopoulos, T., Vlachos, A., Winkels, R., Poulopoulos, A., Betz, H., Deller, T., Brose, N., Varoqueaux, F., and Schwarzacher, S.W. (2011). Increased dentate gyrus excitability in neuroligin-2-deficient mice in vivo. Cereb. Cortex *21*, 357–367.

Kepecs, A., and Fishell, G. (2014). Interneuron cell types are fit to function. Nature *505*, 318–326.

Krueger-Burg, D., Papadopoulos, T., and Brose, N. (2017). Organizers of inhibitory synapses come of age. Curr. Opin. Neurobiol. *45*, 66–77.

Krystal, J.H., Anticevic, A., Yang, G.J., Dragoi, G., Driesen, N.R., Wang, X.J., and Murray, J.D. (2017). Impaired Tuning of Neural Ensembles and the Pathophysiology of Schizophrenia: A Translational and Computational Neuroscience Perspective. Biol. Psychiatry *81*, 874–885.

Lee, E., Lee, J., and Kim, E. (2017). Excitation/Inhibition Imbalance in Animal Models of Autism Spectrum Disorders. Biol. Psychiatry *81*, 838–847.

Liang, J., Xu, W., Hsu, Y.T., Yee, A.X., Chen, L., and Südhof, T.C. (2015). Conditional neuroligin-2 knockout in adult medial prefrontal cortex links chronic changes in synaptic inhibition to cognitive impairments. Mol. Psychiatry *20*, 850–859.

Longo-Guess, C.M., Gagnon, L.H., Cook, S.A., Wu, J., Zheng, Q.Y., and Johnson, K.R. (2005). A missense mutation in the previously undescribed gene Tmhs underlies deafness in hurry-scurry (hscy) mice. Proc. Natl. Acad. Sci. USA *102*, 7894–7899.

Nakamura, Y., Morrow, D.H., Modgil, A., Huyghe, D., Deeb, T.Z., Lumb, M.J., Davies, P.A., and Moss, S.J. (2016). Proteomic Characterization of Inhibitory Synapses Using a Novel pHluorin-tagged γ-Aminobutyric Acid Receptor, Type A (GABAA), α2 Subunit Knock-in Mouse. J. Biol. Chem. *291*, 12394–12407.

Olsen, R.W., and Sieghart, W. (2008). International Union of Pharmacology. LXX. Subtypes of gamma-aminobutyric acid(A) receptors: classification on the basis of subunit composition, pharmacology, and function. Update. Pharmacol. Rev. *60*, 243–260.

Parente, D.J., Garriga, C., Baskin, B., Douglas, G., Cho, M.T., Araujo, G.C., and Shinawi, M. (2017). Neuroligin 2 nonsense variant associated with anxiety, autism, intellectual disability, hyperphagia, and obesity. Am. J. Med. Genet. A. *173*, 213–216.

Petit, M.M.R., Schoenmakers, E.F.P.M., Huysmans, C., Geurts, J.M.W., Mandahl, N., and Van de Ven, W.J.M. (1999). LHFP, a novel translocation partner gene of HMGIC in a lipoma, is a member of a new family of LHFP-like genes. Genomics *57*, 438–441.

Pettem, K.L., Yokomaku, D., Luo, L., Linhoff, M.W., Prasad, T., Connor, S.A., Siddiqui, T.J., Kawabe, H., Chen, F., Zhang, L., et al. (2013). The specific α-neurexin interactor calsyntenin-3 promotes excitatory and inhibitory synapse development. Neuron *80*, 113–128.

Poulopoulos, A., Aramuni, G., Meyer, G., Soykan, T., Hoon, M., Papadopoulos, T., Zhang, M., Paarmann, I., Fuchs, C., Harvey, K., et al. (2009). Neuroligin 2 drives postsynaptic assembly at perisomatic inhibitory synapses through gephyrin and collybistin. Neuron *63*, 628–642.

Sassoè-Pognetto, M., and Patrizi, A. (2013). Development of Glutamatergic and GABAergic Synapses. In Handbook of the Cerebellum and Cerebellar Disorders, M. Manto, D. Gruol, J. Schmahmann, N. Koibuchi, and F. Rossi, eds. (Springer), pp. 237–255.

Shen, K., and Scheiffele, P. (2010). Genetics and cell biology of building specific synaptic connectivity. Annu. Rev. Neurosci. *33*, 473–507.

Sheng, M., and Kim, E. (2011). The postsynaptic organization of synapses. Cold Spring Harb. Perspect. Biol. *3*, a005678.

Siddiqui, T.J., and Craig, A.M. (2011). Synaptic organizing complexes. Curr. Opin. Neurobiol. *21*, 132–143.

Südhof, T.C. (2008). Neuroligins and neurexins link synaptic function to cognitive disease. Nature *455*, 903–911.

Sumita, K., Sato, Y., Iida, J., Kawata, A., Hamano, M., Hirabayashi, S., Ohno, K., Peles, E., and Hata, Y. (2007). Synaptic scaffolding molecule (S-SCAM) membrane-associated guanylate kinase with inverted organization (MAGI)-2 is associated with cell adhesion molecules at inhibitory synapses in rat hippocampal neurons. J. Neurochem. *100*, 154–166.

Sun, C., Cheng, M.C., Qin, R., Liao, D.L., Chen, T.T., Koong, F.J., Chen, G., and Chen, C.H. (2011). Identification and functional characterization of rare mutations of the neuroligin-2 gene (NLGN2) associated with schizophrenia. Hum. Mol. Genet. *20*, 3042–3051.

Takahashi, H., Katayama, K., Sohya, K., Miyamoto, H., Prasad, T., Matsumoto, Y., Ota, M., Yasuda, H., Tsumoto, T., Aruga, J., and Craig, A.M. (2012). Selective control of inhibitory synapse development by Slitrk3-PTPδ trans-synaptic interaction. Nat. Neurosci. *15*, 389–398, S1–S2.

Tanabe, Y., Naito, Y., Vasuta, C., Lee, A.K., Soumounou, Y., Linhoff, M.W., and Takahashi, H. (2017). IgSF21 promotes differentiation of inhibitory synapses via binding to neurexin2α. Nat. Commun. *8*, 408.

Tatti, R., Haley, M.S., Swanson, O.K., Tselha, T., and Maffei, A. (2017). Neurophysiology and Regulation of the Balance Between Excitation and Inhibition in Neocortical Circuits. Biol. Psychiatry *81*, 821–831.

Traynelis, S.F., Wollmuth, L.P., McBain, C.J., Menniti, F.S., Vance, K.M., Ogden, K.K., Hansen, K.B., Yuan, H., Myers, S.J., and Dingledine, R. (2010). Glutamate receptor ion channels: structure, regulation, and function. Pharmacol. Rev. *62*, 405–496.

Tyagarajan, S.K., and Fritschy, J.M. (2014). Gephyrin: a master regulator of neuronal function? Nat. Rev. Neurosci. *15*, 141–156.

Varoqueaux, F., Jamain, S., and Brose, N. (2004). Neuroligin 2 is exclusively localized to inhibitory synapses. Eur. J. Cell Biol. *83*, 449–456.

Varoqueaux, F., Aramuni, G., Rawson, R.L., Mohrmann, R., Missler, M., Gottmann, K., Zhang, W., Südhof, T.C., and Brose, N. (2006). Neuroligins determine synapse maturation and function. Neuron *51*, 741–754.

Wöhr, M., Silverman, J.L., Scattoni, M.L., Turner, S.M., Harris, M.J., Saxena, R., and Crawley, J.N. (2013). Developmental delays and reduced pup ultrasonic vocalizations but normal sociability in mice lacking the postsynaptic cell adhesion protein neuroligin2. Behav. Brain Res. *251*, 50–64.

Woo, J., Kwon, S.K., Nam, J., Choi, S., Takahashi, H., Krueger, D., Park, J., Lee, Y., Bae, J.Y., Lee, D., et al. (2013). The adhesion protein IgSF9b is coupled to neuroligin 2 via S-SCAM to promote inhibitory synapse development. J. Cell Biol. *201*, 929–944.

Yamasaki, T., Hoyos-Ramirez, E., Martenson, J.S., Morimoto-Tomita, M., and Tomita, S. (2017). GARLH Family Proteins Stabilize $GABA_A$Receptors at Synapses. Neuron *93*, 1138–1152.e6.

Zhang, B., Chen, L.Y., Liu, X., Maxeiner, S., Lee, S.J., Gokce, O., and Südhof, T.C. (2015). Neuroligins Sculpt Cerebellar Purkinje-Cell Circuits by Differential Control of Distinct Classes of Synapses. Neuron *87*, 781–796.